Incorporation and localization of substitutional Mn^{2+} ions in cubic ZnS quantum dots

S. V. Nistor,[1] M. Stefan,[1] L. C. Nistor,[1] E. Goovaerts,[2] and G. Van Tendeloo[3]
[1]*National Institute of Materials Physics, P.O. Box MG-7, Magurele-Ilfov, 077125 Romania*
[2]*Department of Physics–ECMP, University of Antwerp, Universiteitsplein 1, 2610 Antwerp, Belgium*
[3]*EMAT–University of Antwerp, Groenenborgerlaan 171, 2020 Antwerp, Belgium*
(Received 6 October 2009; revised manuscript received 4 December 2009; published 29 January 2010)

Multifrequency electron paramagnetic resonance (EPR) and high resolution transmission electron microscopy (HRTEM) investigations were performed on small (2 nm) cubic ZnS nanocrystals (quantum dots–QDs) doped with 0.2% mol Mn^{2+}, self-assembled into a mesoporous structure. The EPR data analysis shows that the substitutional Mn^{2+} ions are localized at Zn^{2+} sites subjected to a local axial lattice distortion, resulting in the observed zero-field-splitting parameter $|D|=41\times10^{-4}$ cm^{-1}. The local distortion is attributed to the presence in the second shell of ligands of a stacking fault or twin, which alters the normal stacking sequence of the cubic structure. The HRTEM results confirm the presence of such extended planar defects in a large percentage of the investigated QDs, which makes possible the proposed substitutional Mn^{2+} impurity ions localization model. Based on these results it is suggested that the high doping levels of Mn^{2+} ions observed in cubic ZnS and possible in other II-VI semiconductor QDs prepared at low temperatures can be explained by the assistance of the extended lattice defects in the impurities incorporation.

DOI: 10.1103/PhysRevB.81.035336 PACS number(s): 61.72.uj, 61.72.Nn, 68.37.Og, 76.30.Fc

I. INTRODUCTION

Dopants play a key role in providing alternative means for controlling the remarkable properties of the semiconducting nanocrystals. In the case of the nanocrystalline II-VI semiconductors prepared at relatively low temperatures (<350 °C), where the diffusion of the impurities into the crystal matrix is not likely to occur, the mechanisms responsible for the observed incorporation of relatively large concentrations of impurity ions, such as Mn^{2+} or Co^{2+}, are still hotly debated.[1,2] In such cases, the success of doping depends on the possibility of the impurity to be adsorbed on the nanocrystals surface and to stay there a time long enough to be incorporated during the growth. Calculations have shown[2] that in perfect crystals, the impurity binding energy depends strongly on the crystallographic orientation of the reconstructed surfaces. It means that for very small (<3 nm) nanocrystallites (quantum dots—QDs), which generally do not exhibit well-defined facets, the doping levels should drop sharply, contrary to experimental observations.[3] The situation is even worse if one considers that for very small cubic nanocrystals, such as CdSe, the formation energy of substitutional Mn^{2+} impurities increases dramatically with nanocrystal size decrease.[4] In all cases, the role of the extended lattice defects has been neglected based on the idea of a high perfection of the nanocrystals, an assumption[4] that our results do not support, at least in the case of cubic ZnS nanocrystals.

In this work, we demonstrate, from correlated multifrequency electron paramagnetic resonance (EPR) and high resolution transmission electron microscopy (HRTEM) investigations of manganese doped cubic ZnS (cZnS:Mn) QDs, that substitutional Mn^{2+} impurities are localized at cation sites subjected to an axial distortion, which is attributed to the presence of a neighboring extended planar lattice defect, as a stacking fault or twin. It is further proposed that such a localization of the Mn^{2+} ions, which seems to occur in other cubic II-VI semiconductor QDs as well, could be due to an active role of the extended lattice defects in the impurities incorporation. This could also explain the relatively high doping levels of the Mn^{2+} ions observed in such QDs prepared by colloidal growth at low temperatures.[2]

II. EXPERIMENTAL

A. Sample preparation

We have investigated a sample of small (2 nm average size) cubic ZnS nanocrystals doped with 0.2% mol Mn^{2+}, taken from a batch prepared at room temperature (RT) by a surfactant-assisted liquid-liquid reaction.[5] The preparation procedure, as well as the results of preliminary structural, *X*-band EPR and optical characterization were reported in Ref. 6. According to the microstructural investigations, the cZnS:Mn batch consists of small nanocrystals of ZnS with cubic (sphalerite) structure of ~2 nm average size, self-assembled into a mesoporous structure of high crystallinity, with a narrow size distribution of crystallites and pores.

B. EPR measurements

The *X* (9.8 GHz)-band EPR measurements were performed with a continuous-wave (CW) type EMX-plus spectrometer from Bruker previously employed for the investigation of the EPR properties of the Mn^{2+} ions in ZnS single crystals with pure cubic structure.[7] A detailed description of the instrument and magnetic field calibration procedures were given in the same paper. The *W*-band EPR measurements were performed with a Bruker E600 spectrometer with a microwave bridge and cylindrical cavity operating in the CW mode at 94 GHz, equipped with a split-coil superconducting magnet (Oxford) mounted on a rotating base. The magnetic field calibration at the sample was made with DPPH (1,1-diphenyl-2-picryl hydrazyl) and a Mn^{2+} doped polycrystalline CaO reference sample, respectively. All EPR measurements were performed at RT.

 ©2010 The American Physical Society

The powdery cZnS:Mn samples for the *X*- and *W*-band measurements were inserted into 3.0 and 0.5 mm i.d. sample tubes, respectively, with one end closed, made from pure silica. The sample thermal treatment was carried out by inserting the sample tubes into a temperature stabilized (± 1 degree) furnace for 15 min, at temperatures which were increased in steps of 25 °C. After each annealing step the EPR spectrum was recorded at RT, in order to monitor the intensity/concentration variation in the Mn^{2+} centers.

The spin Hamiltonian (SH) parameters were determined by fitting the experimental spectra with lineshape simulations performed with the SIM specialized program graciously provided by H. Weihe of the University of Copenhagen and the EPRNMR v.6.4 program (Department of Chemistry, University of Saskatchewan, Canada).

C. TEM measurements

The samples for TEM analysis were prepared by ultrasonically dispersing in ethanol parts of the cZnS:Mn sample previously investigated by EPR spectroscopy and retaining a drop of the colloid on holey carbon covered microscope grids. The observations were carried out with a JEOL 200 CX instrument for conventional TEM and a JEOL 4000 EX instrument for high resolution electron microscopy determinations. The image processing was carried out with the Adobe Photoshop v7.0 software.

III. EPR INVESTIGATION

EPR spectroscopy can accurately determine the exact location of the paramagnetic impurities in the crystal lattice and the resulting small changes in the neighboring ligands configuration, offering insights into the incorporation mechanisms as well.[8] In the case of the cZnS:Mn nanocrystals, one of the most popular materials for optoelectronic applications, the examination of the reported data[9–14] evidences unclear aspects concerning the impurity localization in the nanocrystals lattice. Thus, in the spin Hamiltonian describing the EPR spectrum of the substitutional Mn^{2+} ions, besides the Zeeman and hyperfine interaction terms with parameter values centered around $g=2.002$ and $|A|=64\times 10^{-4}$ cm^{-1}, close to those found in cubic ZnS single crystals,[7] some authors have also included noncubic zero-field splitting (ZFS) terms. The reported parameter values are spread over a two orders of magnitude range. Moreover, the corresponding presence of a local noncubic crystal lattice deformation at the substitutional Zn^{2+} site, known from EPR studies on cubic $ZnS:Mn^{2+}$ single crystals[7] to exhibit a local cubic (T_d) symmetry, has not been explained. We believe this situation is mainly due to the low accuracy of the previous SH parameters determinations.

Our early *X*-band EPR investigation revealed the presence in the cZnS:Mn QDs of a substitutional Mn^{2+} center, called Mn^{2+}(I), and of two surface centers, called Mn^{2+}(II) and Mn^{2+}(III).[6] From pulse annealing experiments we found out that the Mn^{2+}(III) centers transform into Mn^{2+}(II) centers during heating, by the temperature activated desorption of water molecules from the nanocrystals surface.[15] Fig. 1 shows the simpler *X*- and *W*-band EPR spectra obtained from a cZnS:Mn sample annealed for 30 min at 175 °C, where only the Mn^{2+}(I) and Mn^{2+}(II) centers are present. The transition fields attributed to the remaining Mn^{2+}(I) and Mn^{2+}(II) centers are marked with vertical lines, namely, six allowed (M_s: $-1/2 \leftrightarrow 1/2, \Delta M_I=0$) and 10 forbidden ($M_s$: $-1/2 \leftrightarrow 1/2, \Delta M_I=\pm 1$) hyperfine transitions for the Mn^{2+}(I) centers and six allowed hyperfine transitions for the Mn^{2+}(II) centers. As expected, the two spectra are better separated in the *W* band. Moreover, the forbidden transitions of the Mn^{2+}(I) centers are practically unobservable at such a high frequency, as the intensity ratio of the forbidden vs allowed hyperfine transitions I_f/I_a is known[8] to be proportional to $(D/B)^2$.

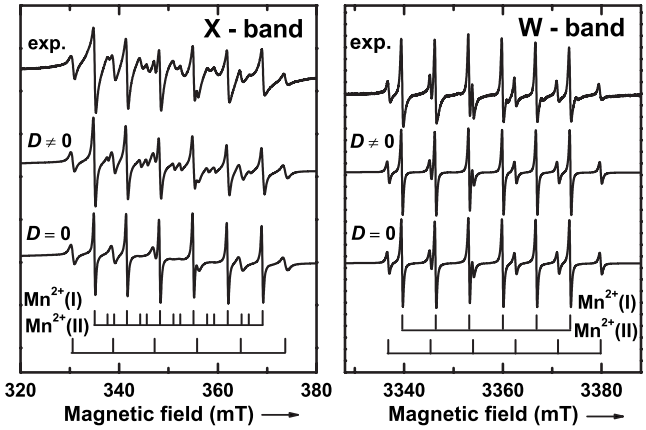

FIG. 1. The experimental *X* (9.87 GHz)- and *W* (94.06 GHz)-band EPR spectra of a mesoporous ZnS:Mn sample pulse annealed up to +175 °C (exp) and the corresponding simulated spectra as a sum of the Mn^{2+}(I) and Mn^{2+}(II) spectra simulations without ($D=0$) and with the axial ZFS term included ($D\neq 0$). The transition fields of the Mn^{2+}(I) and Mn^{2+}(II) centers are marked with vertical lines. The less accurate fit of the central part of the *X*-band spectrum is due to the overlap with lines from an unidentified paramagnetic species.

In the present research we have been able to determine with higher accuracy, from *X* (9.8 GHz)- and *W* (94 GHz)-band EPR measurements, the SH parameters, including the presence and magnitude of the ZFS terms describing the local noncubic deformation at substitutional Zn^{2+} site and to explain their origin, using data from early EPR investigations on highly defective ZnS single crystals, as well as the results of our HRTEM investigations.

The EPR spectra of the Mn^{2+} centers in nanocrystalline cZnS:Mn are described by the following spin Hamiltonian, with usual notations:[8]

$$H = g\mu_B \vec{S}\cdot\vec{B} + A\vec{S}\cdot\vec{I} + \frac{a}{6}\left[(S_x^4+S_y^4+S_z^4) + \frac{1}{5}S(S+1)(3S^2 + 3S - 1)\right] + + D\left[S_z^2 - \frac{1}{3}S(S+1)\right] + \mu_N g_N \vec{B}\cdot\vec{I}. \quad (1)$$

Here, the first two terms represent the main interactions of the $S=5/2$ electron spin with the external magnetic field *B* (the electron Zeeman interaction) and the hyperfine interac-

TABLE I. The SH parameters at RT for substitutional Mn^{2+} ions in cZnS QDs determined in this work in comparison with some previously reported values in ZnS nanocrystals and single crystals. The hyperfine A and ZFS parameters a and D are given in $[10^{-4}\ \mathrm{cm}^{-1}]$ units.

Lattice host/center	g	A	$\lvert D\rvert$	a
cZnS:Mn QDs/center Mn^{2+}(I) [a]	2.0022	−63.70	41	7.987
	±0.0001	±0.05	±3	
cZnS:Mn QDs /center NC1 [b]	2.003	−64.5		
cZnS: Mn QDs/center SI [c]	2.0010	−63.9	1.0	
cZnS:Mn QDs/center I [d]	2.0024	−64.5	91.0	
cZnS:Mn QD-samples 1 and 2 [e]	g_{xx}=2.0064	A_{xx}=−63.9	37.4	
	g_{yy}=2.0064	A_{yy}=−64.0	$\lvert E\rvert$=12.47	
	g_{zz}=2.0066	A_{zz}=−64.4		
cZnS:Mn QDs/center Ib [f]	$g_{\perp}$=2.0075	$A_{\perp}$=−63.8	37.4	
	$g_{\parallel}$=2.0040	$A_{\parallel}$=−65.2	$\lvert E\rvert$=12.47	
cZnS:Mn single crystal/subst. Mn^{2+} [g]	2.00225	−63.88	0	7.987
Mixed polytype ZnS:Mn crystal/center PN [h]	2.0018	−64.9	36.1	7.35
				a-F=7.4

[a]This work; a-parameter value was taken in agreement with Ref. 7.
[b]Reference 9.
[c]Reference 10.
[d]References 11 and 12.
[e]Reference 13.
[f]Reference 14.
[g]Reference 7.
[h]References 17–19.

tion with the $I=5/2$ nuclear spin of the ^{55}Mn (100% abundance) isotope, respectively. The next two terms describe the interaction of the electron spin with the local crystal field, characterized by the ZFS cubic a and axial D parameters, and the last one corresponds to the nuclear Zeeman interaction of the $I=5/2$ nuclear spin with the external magnetic field B. Table I presents the previously reported parameter values of the substitutional Mn^{2+} ions in cubic ZnS nanocrystals[9–14] and single crystals,[7,15–19] which are of interest in this investigation. The SH parameters were generally determined by simply fitting the calculated line positions/shapes of the central allowed transitions with experimental data at one frequency.

Highly accurate SH parameter values for the Mn^{2+}(I) center in the cZnS:Mn QDs were presently obtained (Table I) by fitting the low and high frequency experimental EPR spectra with line shape simulations which took into consideration the hyperfine forbidden transitions and the line broadening effects, both strongly influenced by the noncubic ZFS terms. The increased accuracy also resulted from the higher resolution of our EPR spectra due to the narrower lines (0.4 mT linewidth in the X band, as compared to the best reported value[11] of 0.6 mT). One should mention that no further improvement in the spectra resolution was observed by decreasing the measuring temperature down to 40 K.

The SH parameters determination procedure consisted of two steps. In a first step, accurate g and A parameters, very close to those found in cubic ZnS single crystals[7] were determined by fitting the W-band spectrum with the calculated line positions obtained by neglecting the contribution of the ZFS terms, which is within the experimental errors at such high magnetic fields. Further on, the axial ZFS parameter $\lvert D\rvert=(41\pm3)\times10^{-4}\ \mathrm{cm}^{-1}$ value was obtained by fitting the experimental lineshape of the more sensitive X-band spectrum using the previously determined g and A values.

The quality of the fitting with experimental spectra (see Fig. 1) demonstrates that the Mn^{2+}(I) EPR spectra are well described by the SH [Eq. (1)] which includes, besides the cubic terms with g, a, and A values very close to those found in cZnS single crystals, the axial ZFS term. The SH parameters of the Mn^{2+}(II) center resulting from the same procedure were: $g=2.0012\pm0.0001$, $A=-(80.5\pm0.1)\times10^{-4}\ \mathrm{cm}^{-1}$, and $10\times10^{-4}\ \mathrm{cm}^{-1}<\lvert D\rvert<70\times10^{-4}\ \mathrm{cm}^{-1}$. The simulated spectra from Fig. 1 are the sum of the calculated spectra of the Mn^{2+}(I) and Mn^{2+}(II) centers. The line broadening effects were included as fluctuations in the ZFS parameter values.

Due to the local strain induced broadening of the EPR lines, it was not possible to accurately determine the smaller fourth order ZFS parameter a. Therefore, the single crystal value of the a parameter, which changes only slightly between the various ZnS crystalline phases[7,15–19] was used throughout the calculations. To underline the necessity and importance of including the axial ZFS term in the spectra simulation in order to accurately reproduce the experimental X-band spectrum including the forbidden transitions, we included in Fig. 1 the results of simulations with and without this term.

According to our simulations, a possible contribution from a sizable amount of substitutional Mn^{2+} ions at pure

unperturbed cubic sites which, due to the close *g*- and *A*-parameter values, would be hidden under the spectrum of the Mn^{2+}(I) centers, can be excluded. Indeed, in the absence of noncubic ZFS terms in the SH of such centers, the intensity of the forbidden lines would be negligible (see the *X*-band spectrum simulation with $D=0$ from Fig. 1), resulting in a smaller total relative intensity of the forbidden transitions than actually observed in our experimental *X*-band spectrum.

The lattice distortion at the substitutional Mn^{2+} ions in the investigated cZnS:Mn QDs, resulting in the observed axial ZFS term, seems very likely to be due to a neighboring defect, either as an unintentional impurity, or as an intrinsic lattice defect. A neighboring impurity should be excluded, because the estimated 200 ppm concentration of Mn^{2+} ions in the investigated sample is too high compared to the trace impurity levels in the starting materials. Neighboring intrinsic point defects as double charged vacancy/interstitials cannot be totally excluded, but they are also unlikely, in view of the similar electrical charges and close radii of the Mn^{2+} impurity and substituted Zn^{2+} cation. Therefore, we have to consider the presence of a neighboring extended lattice defect as the source of the local noncubic distortion.

Stacking faults and twins are the common extended defects in materials which crystallize in both sphalerite (cubic) and wurtzite (hexagonal) closed packed structures.[20,21] The major difference between the two polytypes is the stacking sequence of the planes along a $\langle 111 \rangle$ direction in the sphalerite structure, which corresponds to the *c* axis of the wurtzite structure. In fact both structures are very similar: they only differ in the third nearest-neighbor atomic arrangement, i.e., at the third stacking layer. In crystals with sphalerite structure, planar defects such as stacking faults and twins occur along the $\{111\}$ planes.

The presence of extended defects next to Mn^{2+} ions has been reported in EPR studies on ZnS:Mn single crystals grown at high temperatures from melt, where the wurtzite phase is stable.[17–19] Such crystals exhibit after cooling down to RT a mixed structure, containing regions of various polytype structures and many extended defects as stacking faults and twins. Thus, besides the known EPR spectra from Mn^{2+} ions in regions with cubic[7] and hexagonal[16] structure, an additional spectrum from the Mn^{2+} ions subjected to a local axial (trigonal) crystal field along the $\langle 111 \rangle$ axis in sphalerite (equivalent to wurtzite *c* axis) characterized by $|D|=36.1 \times 10^{-4}$ cm^{-1}, called the trigonal PN center, has been identified.[17–19] The PN center was attributed to substitutional Mn^{2+} ions at Zn^{2+} sites where the normal stacking sequence of layers along the sphalerite $\langle 111 \rangle$ axis was changed by the gliding of the neighboring ligands plane due to a stacking fault or twin. From the close values of the axial ZFS parameter *D* one concludes that a similar situation occurs in the cZnS:Mn QDs; the substitutional Mn^{2+} impurity is localized in a $\{111\}$ layer, which contains the Mn^{2+} ion with its tetrahedrally coordinating sulfur ligands, lying next to a stacking fault or twin. The small difference in the SH parameters of the Mn^{2+}(I) centers in the cZnS:Mn QDs and in the ZnS mixed phase single crystals (see Table I) is attributed to differences in the arrangement of the first neighboring ligands for the corresponding structures and to experimental errors.

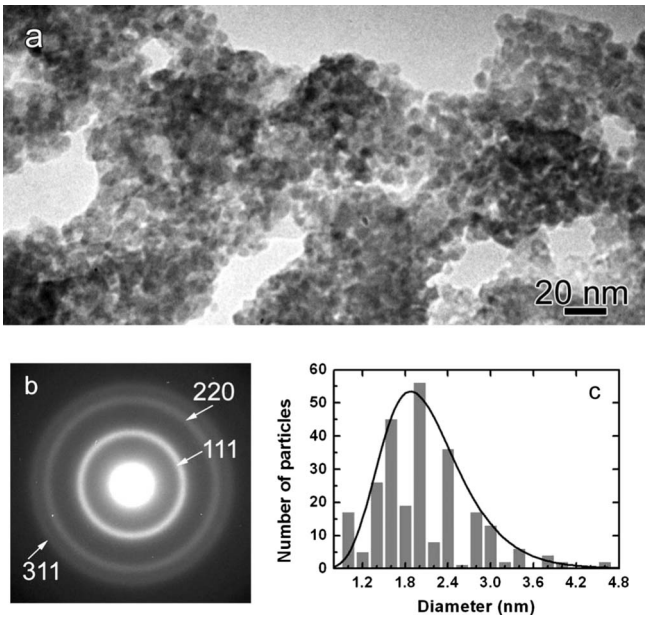

FIG. 2. (a) TEM image revealing the mesoporous morphology of the cZnS:Mn QDs sample. (b) The corresponding electron diffraction pattern indexed with the cubic (sphalerite) ZnS structure. (c) Histogram showing the size distribution of the cZnS:Mn crystallites.

One should mention that although the possibility of another configuration of defects next to the Mn^{2+} impurity ions in the cZnS:Mn QDs cannot be excluded, it is very unlikely that it would result in SH parameter values and local symmetry similar to those presently reported.

To confirm the proposed localization of the substitutional Mn^{2+} ions in the cZnS:Mn QDs, we employed HRTEM to determine the presence and nature of the extended defects in the investigated nanocrystals.

IV. MICROSTRUCTURAL (TEM/HRTEM) INVESTIGATION

The microstructure of the particular cZnS:Mn sample investigated by multifrequency EPR has been also examined by conventional TEM. Figure 2(a) reveals the mesoporous structure of the specimen with a spongelike morphology, as previously observed in pure mesoporous ZnS samples.[5] The pore walls are constituted from cross-linked nm-sized ZnS crystallites, of rather uniform round shapes. The corresponding electron diffraction pattern, Fig. 2(b), has been indexed based on the cubic structure of ZnS.

The size distribution of the cZnS nanocrystallites has been also determined from the TEM data. Figure 2(c) shows the histogram obtained by measuring the diameter/size of 259 nanocrystallites on several TEM images. The calculated average diameter is $d_m=(2.1 \pm 0.3)$ nm. The rather large estimated error results from the difficulty in determining the size of each nanocrystallite in the agglomerates. The size distribution histogram has been fitted with a log-normal function. From this fit, we determined the statistical mean particle diameter $d_m=(2.03 \pm 0.5)$ nm, close to the calculated value,

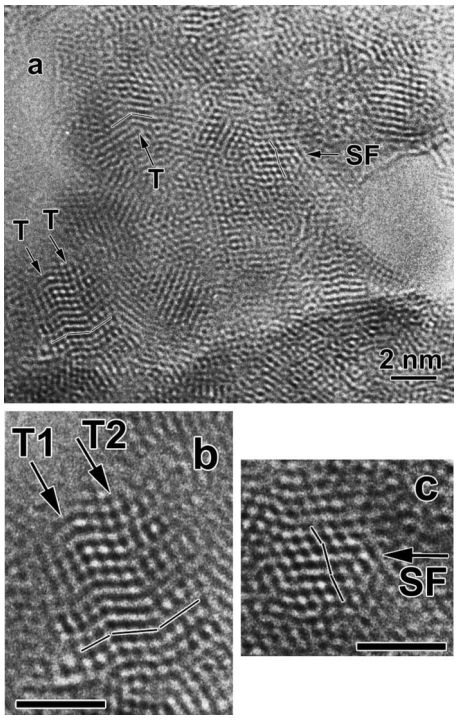

FIG. 3. (a) HRTEM image of the cZnS:Mn QDs sample revealing in some crystallites (marked by arrows) planar defects such as twin interfaces (t) and stacking faults (SF). (b) and (c) enlarged HRTEM images of crystallites oriented along the [110] zone axis showing the atomic structure of these defects. The black lines are drawn to guide the eye. Scale bars: 2 nm.

and the geometrical standard deviation of $\sigma = 1.3 \pm 0.1$

To reveal the stacking defects in the cubic ZnS:Mn nanoparticles we performed HRTEM observations. The atomic structure of extended defects can be imaged by HRTEM only if the defects exhibit translation symmetry along the viewing direction. For crystals with sphalerite structure this condition is fulfilled along the [110] viewing direction.

Figure 3(a) shows a HRTEM image of a very thin part of a ZnS:Mn sample where the particles are not superposed. Some of the cZnS:Mn nanocrystals exhibit defects such as twins (T) or stacking faults (SF), marked by arrows. Enlarged images of the crystallites well oriented along [110] are presented in Figs. 3(b) and 3(c). The cZnS:Mn nanocrystal from Fig. 3(b) exhibits two twin interfaces, marked by arrows. In the case of twinning, the normal stacking sequence along the (111) planes is disturbed on a single layer of atom columns, which forms the coherent twin (or mirror) plane. A careful examination of both twins shows that they exhibit steps, introduced by twinning dislocations.[22] This is more evident on the twin interface marked T2, which has a wavy aspect. Figure 3(c) reveals the atomic structure of an intrinsic stacking fault in a cZnS:Mn nanocrystallite. In this case, the stacking sequence of the (111) planes is disturbed over three atomic layers. In fact, the stacking of these three planes turns from cubic close packed into hexagonal close packed. Any substitutional impurity localized in these atomic planes will be in a distorted neighborhood, with regard to the perfect cubic lattice.

Examining several HRTEM images, we also found out that many (~30%) of the cZnS:Mn crystallites oriented along [110] contain planar extended defects in the form of stacking faults and twins. Considering that the ZnS:Mn nanocrystallites are arbitrarily oriented in the investigated sample, it results that a large fraction of them contain such extended defects. The observation of the extended defects by HRTEM confirms the simulation results based on a Debye function analysis, which has shown[10] that the presence in the ZnS:Mn nanocrystals of extended defects in the form of twins is essential for fitting the experimental XRD patterns. One should also mention that because the ZnS nanocrystals are small, the twins and stacking faults intersect their surface, giving rise to surface steps and dislocations.

V. DISCUSSION AND CONCLUSIONS

The presence of the extended planar defects observed by HRTEM in the investigated cZnS:Mn QDs offers additional support for the proposed localization of the substitutional Mn^{2+} ions next to a stacking fault or twin, which is perturbing the surrounding lattice by lowering the local T_d symmetry at the impurity site. The presence of forbidden hyperfine transitions, which can be also observed in the EPR spectra of substitutional Mn^{2+} ions in CdS (Ref. 23) and ZnSe (Ref. 24) nanocrystals, reflects a lower local symmetry at impurity in these cubic nanocrystals as well. Therefore, it is reasonable to assume that the localization of the substitutional Mn^{2+} ions next to extended planar defects could be a general characteristic for the small cubic II-VI semiconductor QDs.

The proposed localization of the substitutional Mn^{2+} in the II-VI semiconductor QDs next to an extended lattice defect has some important implications. First, the resulting local axial distortion observed in the EPR spectra should be taken into consideration when evaluating the local quantum properties. Second, the absence of a sizable amount of substitutional Mn^{2+} ions at unperturbed purely cubic (T_d) cation sites in the cubic ZnS QDs strongly suggests that the extended planar defects play an essential role in the incorporation of Mn^{2+} impurity ions in relatively large concentrations, during preparation at low temperatures, a phenomenon which cannot be explained by the presently accepted mechanisms of doping.[1,2] According to these mechanisms[1,2] the success in doping such nanocrystals depends on the possibility of the impurity to be adsorbed on the nanocrystals surface and to stay there a time long enough to be incorporated during the growth process. The size and shape of the nanocrystals play an important role. Calculations show[2] that the impurity binding energy strongly depends on the crystallographic orientation of the reconstructed surfaces. Consequently, crystallites with well defined facets are necessary to ensure a diffusion assisted doping process. However, in the case of small nanocrystals (<3 nm), where no such specific surfaces are observed, doping based on such a mechanism would be difficult, which contradicts the experimental results.

Based on our present results, the assistance of the extended defects in the adsorption process could be a valid solution to explain the doping of small cubic ZnS nanocrystals. Indeed, it is a well known experimental fact that defects, such as steps on the surfaces or dislocations, which emerge

when the extended planar defects intersect the nanocrystallite surface, are "attracting" impurities,[25] possibly by lowering their binding energy. Therefore, one expects the doping to be controlled mainly by the trapping of impurities at the steps and dislocations at the surface of the growing QDs containing stacking defects.

The large fraction of planar extended defects observed in the investigated cZnS:Mn QDs makes possible the relatively high fraction of the Mn^{2+} impurities observed in the investigated sample and the formation of impurity aggregated states at higher dopant concentrations, as previously reported in cZnS:Mn nanocrystals of comparable size.[10–12,14] One should also mention that according to such incorporation model, at higher dopant concentrations one expects the impurities to aggregate preferentially in the {111} planes parallel to the extended defects, resulting in specific properties which should be further investigated.

In summary, we have shown that substitutional Mn^{2+} impurity ions are preferentially localized in cZnS and very likely in other cubic II-VI semiconductor QDs, at cation sites subjected to a local axial distortion, which is also expected to influence the local quantum states and resulting optical, electrical and magnetic properties. The axial distortion is attributed to the presence of a neighboring extended planar lattice defect, as a twin or stacking fault. According to available experimental data the high doping level of Mn^{2+} impurity ions in cubic II-VI semiconductor QDs prepared by colloidal growth could be explained by the presence and role of extended lattice defects in the incorporation of impurities, very likely by lowering the binding energy at the surface of the growing nanocrystallite. Further experimental and theoretical work, such as electron-nuclear double resonance investigations and *ab initio* modeling of the ions incorporation in the presence of extended lattice defects, could confirm our conclusions and their validity for other impurity ions in II-VI semiconductor QDs.

ACKNOWLEDGMENTS

We thank C. D. Mateescu for samples preparation and D. Zernescu for technical assistance. The research was supported by project PN-II-ID-PCE under Grant No. 523/2009 financed by UEFISCSU-CNCSIS. Financial support from the Flemish Fund for Scientific Research (FWO-Vlaanderen) under Group Project No. G.0116.06 is also gratefully acknowledged.

[1] D. J. Norris, A. L. Efros, and S. C. Erwin, Science **319**, 1776 (2008).
[2] S. C. Erwin, L. Zu, M. I. Haftel, A. L. Efros, T. A. Kennedy, and D. J. Norris, Nature (London) **436**, 91 (2005).
[3] H. Hu and W. Zhang, Opt. Mater. **28**, 536 (2006).
[4] G. M. Dalpian and J. R. Chelikowsky, Phys. Rev. Lett. **96**, 226802 (2006).
[5] L. C. Nistor, C. D. Mateescu, R. Birjega, and S. V. Nistor, Appl. Phys. A: Mater. Sci. Process. **92**, 295 (2008).
[6] S. V. Nistor, L. C. Nistor, M. Stefan, C. D. Mateescu, R. Birjega, N. Solovieva, and M. Nikl, Superlattices Microstruct. **46**, 306 (2009).
[7] S. V. Nistor and M. Stefan, J. Phys.: Condens. Matter **21**, 145408 (2009).
[8] A. Abragam and B. Bleaney, *Electron Paramagnetic Resonance of Transition Ions* (Clarendon Press, Oxford, 1970).
[9] T. A. Kennedy, E. R. Glaser, P. B. Klein, and R. N. Bhargava, Phys. Rev. B **52**, R14356 (1995).
[10] P. H. Borse, D. Srinivas, R. F. Shinde, S. K. Date, W. Vogel, and S. K. Kulkarni, Phys. Rev. B **60**, 8659 (1999).
[11] T. Igarashi, M. Ihara, T. Kusunoi, K. Ohno, T. Isobe and M. Senna, J. Nanopart. Res. **3**, 51 (2001).
[12] T. Igarashi, T. Isobe, and M. Senna, Phys. Rev. B **56**, 6444 (1997).
[13] P. A. Gonzalez Beermann, B. R. McGarvey, S. Muralidharan, and R. C. W. Sung, Chem. Mater. **16**, 915 (2004).
[14] P. A. Gonzalez Beermann, B. R. McGarvey, and B. O. Skadtchenko, S. Muralidharan, and R. C. W. Sung, J. Nanopart. Res. **8**, 235 (2006).
[15] S. V. Nistor, M. Stefan, L. C. Nistor, C. D. Mateescu, and R. Birjega, J. Nanosci. Nanotechnol. (to be published).
[16] J. Schneider, S. R. Sircar, and A. Rauber, Z. Naturforsch. A **18a**, 980 (1963).
[17] B. Lambert, T. Buch, and B. Clerjaud, Solid State Commun. **10**, 25 (1972).
[18] T. Buch, B. Clerjaud, B. Lambert, and P. Kovacs, Phys. Rev. B **7**, 184 (1973).
[19] J. Kreissl and W. Gehlhoff, Phys. Status Solidi A **81**, 701 (1984)
[20] P. Pirouz and J. W. Yang, Ultramicroscopy **51**, 189 (1993).
[21] H. Zhang and J. F. Banfield, J. Phys. Chem. C **113**, 9681 (2009).
[22] L. C. Nistor, G. Van Tendeloo, and G. Dinca, Phys. Status Solidi A **201**, 2578 (2004)
[23] G. Counio, S. Esnouf, T. Gascoin, and J.-P. Boilot, J. Phys. Chem. **100**, 20021 (1996).
[24] T. J. Norman, D. Magana, Jr., T. Wilson, C. Burns, J. Z. Zhang, D. Cao, and F. Bridges, J. Phys. Chem. B **107**, 6309 (2003).
[25] S. Amelinckx, *Solid State Physics: Advances in Research and Applications*, edited by F. Seitz and D. Turnbull (Academic Press, New York, 1964), Suppl. 6, pp. 55–89.